
Since January 2020 Elsevier has created a COVID-19 resource centre with free information in English and Mandarin on the novel coronavirus COVID-19. The COVID-19 resource centre is hosted on Elsevier Connect, the company's public news and information website.

Research Article

# SARS-CoV-2 Fusion Peptide has a Greater Membrane Perturbating Effect than SARS-CoV with Highly Specific Dependence on $Ca^{2+}$

**Alex L. Lai and Jack H. Freed** *

***ACERT,*** *Department of Chemistry and Chemical Biology, Cornell University, Ithaca, NY 14853, United States*

***Correspondence to Jack H. Freed:*** *jhf3@cornell.edu (J.H. Freed)*
https://doi.org/10.1016/j.jmb.2021.166946
***Edited by Eric O. Freed***

## Abstract

Coronaviruses are a major infectious disease threat, and include the zoonotic-origin human pathogens SARS-CoV-2, SARS-CoV, and MERS-CoV (SARS-2, SARS-1, and MERS). Entry of coronaviruses into host cells is mediated by the spike (S) protein. In our previous ESR studies, the local membrane ordering effect of the fusion peptide (FP) of various viral glycoproteins including the S of SARS-1 and MERS has been consistently observed. We previously determined that the sequence immediately downstream from the S2′ cleavage site is the *bona fide* SARS-1 FP. In this study, we used sequence alignment to identify the SARS-2 FP, and studied its membrane ordering effect. Although there are only three residue differences, SARS-2 FP induces even greater membrane ordering than SARS-1 FP, possibly due to its greater hydrophobicity. This may be a reason that SARS-2 is better able to infect host cells. In addition, the membrane binding enthalpy for SARS-2 is greater. Both the membrane ordering of SARS-2 and SARS-1 FPs are dependent on $Ca^{2+}$, but that of SARS-2 shows a greater response to the presence of $Ca^{2+}$. Both FPs bind two $Ca^{2+}$ ions as does SARS-1 FP, but the two $Ca^{2+}$ binding sites of SARS-2 exhibit greater cooperativity. This $Ca^{2+}$ dependence by the SARS-2 FP is very ion-specific. These results show that $Ca^{2+}$ is an important regulator that interacts with the SARS-2 FP and thus plays a significant role in SARS-2 viral entry. This could lead to therapeutic solutions that either target the FP-calcium interaction or block the $Ca^{2+}$ channel.



## Introduction

Coronaviruses (CoVs) are a major infectious disease threat for humans and animals; examples include SARS-CoV, MERS-CoV, and SARS-CoV-2[1] (SARS-1, MERS and SARS-2 for simplicity). The pandemic outbreaks of severe acute respiratory syndrome (SARS) in 2003 and Middle East respiratory syndrome (MERS) in 2012 caused 774 and 624 deaths worldwide respectively.[1] SARS-2 is the pathogen of the ongoing COVID-19 pandemic, which has severely harmed our public health, economy and social life. The study of SARS-2 is one of the central agendas in an effort to combat the pandemic.

Glycoproteins located on the viral envelope are required to mediate the viral entry into the host cells and it is a major pathogenicity determinant.[2,3] The viral spike protein (S) is such a CoV glycoprotein. Like SARS-1 and MERS, the S protein of SARS-2 consists of S1 and S2 subunits. The two major steps in viral entry are (1) receptor binding, in which the S1 subunit recognizes a receptor on the host cell membrane, e.g., ACE2, and attaches the virus to the host cell, followed by (2) membrane fusion, in which the S2 subunit mediates the viral envelop membrane and the host membrane fusing together and releasing the virion into the host cell. Membrane fusion is a required stage in viral entry[4]; thus, the blocking of this membrane fusion could be

an objective leading to vaccines and therapies to combat COVID-19.[5] The major region of S that interacts with lipid bilayers of the host is called the "fusion peptide" (FP). The FP is critical for membrane fusion, as it inserts into the host lipid bilayer upon activation of the fusion process, perturbing the membrane structure, and initiating the membrane fusion.

Knowledge of the structure and function of the S of SARS-2 is thus important in order to better understand the process of viral transmission, its mechanism and for the development of medical countermeasures (including vaccines, inhibitory peptides, and drugs). The FP is highly conserved across the diverse CoV family, so it serves as a desirable potential target. Although the S protein is categorized as a class I viral fusion protein, it differs in several ways from a typical class I viral fusion protein. Whereas other class I viral fusion proteins such as influenza and HIV glycoproteins are activated via cleavage by host cell proteases at a single site directly adjacent to the fusion peptide, coronaviruses have two distinct cleavage sites (S1/S2 and S2′) that can be activated by a much wider range of proteases, with FP function able to be modulated by changes in the cleavage site position relative to the FP. This gives coronaviruses unique flexibility in their ability to invade new cell types, tissues, and host species.

There is no crystal structure of intact S, severely limiting our mechanistic understanding of coronavirus fusion. While the basic structure of the S of SARS and SARS-2 can be revealed using cryo-EM techniques[6–8] and part of the SARS-2 S2 subunit has been solved by X-ray crystallography,[9,10] many structural and functional aspects remain undetermined, especially since the active form of FPs (i.e., associated with membranes) is generally not determined in the crystallographic structure as they are hydrophobic and intrinsically disordered. ESR is a useful technique to study the effect of FPs on the membrane structure with implications for the mechanism leading to membrane fusion. It can also be used to determine the peptide structure in the membrane in the form of Pulse-Dipolar ESR[11,12] and Power Saturation ESR.[13]

Previously, we used phospholipid (PC) spin labels to detect the perturbation of the membrane by viral FP and TMD.[14–20] We have shown that a wide range of viral FPs induce local membrane ordering, while their inactive mutants do not. We have interpreted this as associated with dehydration induced by the insertion of active FP.[15,17,21] We also found that this membrane ordering effect can be used as a criterion to identify the FP, as in the case of the gametic fusogen HAP2.[20] It was also used to identify the *bona fide* SARS-1 FP as the region immediately following the S2′ cleavage site, since the two other candidates do not induce local membrane ordering as efficiently. In the same study, we showed that the SARS-1 FP consists of FP1 and FP2 domains and that the activity of SARS-1 FP is $Ca^{2+}$ dependent, with its FP1 and FP2 each binding one $Ca^{2+}$ ion.[18] (The boundary between FP1 and FP2 is quite arbitrary as the middle of the FP is a loose linker.[22] In our SARS-1 FP paper,[18] the FP1 and FP2 peptides actually overlapped a little bit. Here, we define the FP1 as 816–833 in SARS-2 and 798–815 in SARS-1, and FP2 as 817–856 in SARS-2 and 816–939 in SARS-1, as shown in Figure 1C.) Based on that finding, we proposed a bipartite model for the SARS-1 FP (Figure 1A, where we have updated the molecular model according to the new MD simulation model for SARS-2 FP[22] and an Heliquest Plot for the first 11 amino acids is shown.[23]). We showed that the MERS-CoV FP also has FP1 and FP2 domains and its activity is also $Ca^{2+}$ dependent, but only FP1 binds one $Ca^{2+}$ ion.[24] This $Ca^{2+}$ dependent fashion is also found in the Ebolavirus (EBOV) FP case.[19] In this study we apply the same methodology on the SARS-2 FP and compare it with the SARS-1 and MERS FP. We found that the SARS-2 FP also induces membrane ordering as the SARS-1 in a $Ca^{2+}$ dependent fashion, but the SARS-2 FP induces even greater membrane ordering ($S_0$) than both the SARS-1 and MERS FP, and its membrane binding energy is higher, possibly due to its greater hydrophobicity.

## Results

### Peptide cloning and expression

We previously identified the *bona fide* SARS-1 FP[25] as the sequence that is immediately downstream of the S2′ cleavage site. Based on the sequence alignment, we hypothesize that the homologous sequence on the SARS-2 S protein is the *bona fide* SARS-2 FP as well. We planned to test this by examining its membrane ordering effect as the criterion as before. We previously cloned the SARS-1 FP gene into a pET41 expression vector containing a T7 promoter. The construct was originally peptide obtained from the Lukas Tamm lab[26] which was used for the expression of the Ebolavirus FP, and we have replaced the Ebolavirus FP gene with the WT SARS-1 FP gene sequence for our SARS-1 FP expression. We have also been using it to generate SARS-1 FP mutants in our SARS-1 FP research. In order to speed our research, we decided to generate the SARS-2 FP from this SARS-1 FP clone. As shown in Figure 1C, three residues are different between the SARS-1 FP and SARS-2 FP. Therefore, we have designed the primers and performed point mutagenesis on these three sites to generates the SARS-2 FP clone. The peptide was expressed in *E. coli* and purified. Figure 2A shows the SDS-PAGE gel of the fractions collected from His-tag column. The size of the peptide is correct. The combined fraction was further

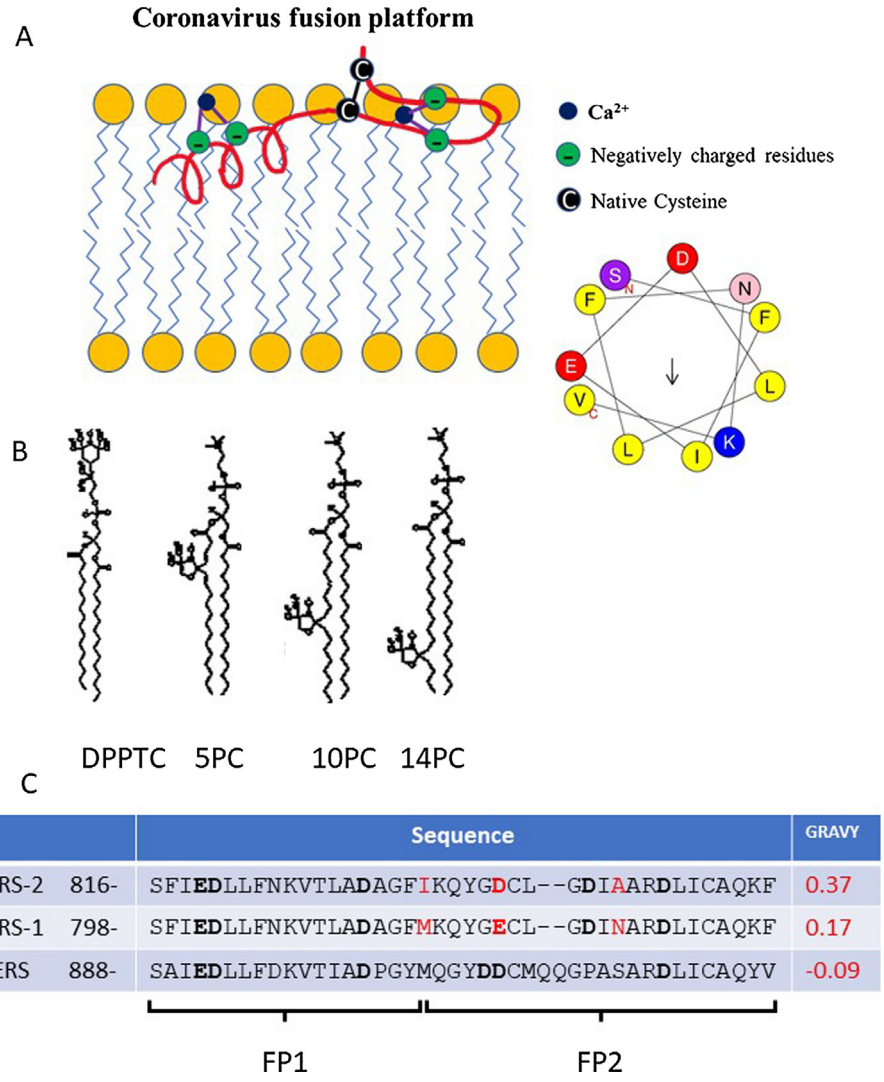


| | | Sequence | GRAVY |
|---|---|---|---|
| SARS-2 | 816- | SFI**ED**LLFNKVTLA**D**AGFIKQYG**D**CL--G**D**IAAR**D**LICAQKF | 0.37 |
| SARS-1 | 798- | SFI**ED**LLFNKVTLA**D**AGFMKQYG**E**CL--G**D**INAR**D**LICAQKF | 0.17 |
| MERS | 888- | SAI**ED**LLFDKVTIA**D**PGYMQGY**DD**CMQQGPASAR**D**LICAQYV | -0.09 |

FP1 FP2

**Figure 1.** (A). A model of the coronavirus FP or "platform" interacting with a lipid bilayer (adopted from our previous model[18] using the structural information from CD spectroscopy in this study, and the molecular dynamics model.[22] A Heliquest Plot[23] for the first 11 amino acids is shown. (B) The structure of spin labeled lipids used: DPPTC, 5PC, 10PC and 14PC. (C) The sequence alignment of SARS-2, SARS-1, and MERS FPs, and their grand average of hydropathy (GRAVY) values (calculated using GRAVY Calculator, http://www.gravy-calculator.de/index.php). The residues in red highlight the difference between SARS-2 and SARS FP. The residues in bold are the negatively charged residues which are potential $Ca^{2+}$ binding sites.

purified using size-exclusion chromatography. The size of the peptide was further validated by mass spectroscopy. All the data presented in this study are from this expressed version. We received synthesized SARS-2 FP from Biomatik USA LLC (Wilmington, DE) at a later time and have repeated some key experiments (CD, ESR and ITC), finding that the results between the expressed and synthesized ones are nearly identical. We used POPC/POPG/Chol = 3/1/1 as the model membrane system. POPG is an anionic lipid and the POPC/POPG mixture is widely used in other fusion peptide research.[27,28]

## Circular dichroism spectroscopy (CD)

To determine whether the SARS-2 FP interacts with membrane, circular dichroism (CD) spectroscopy was used to determine the secondary structures of the peptides in solution and in membranes, which allows us to compare the structural transitions occurring between these two environments. As shown in Figure 2B, whereas the FP exhibits mostly a random coil structure in solution, it adopts a mixture of alpha-helix, beta-sheet and random-coil secondary structures in the presence of small unilamellar

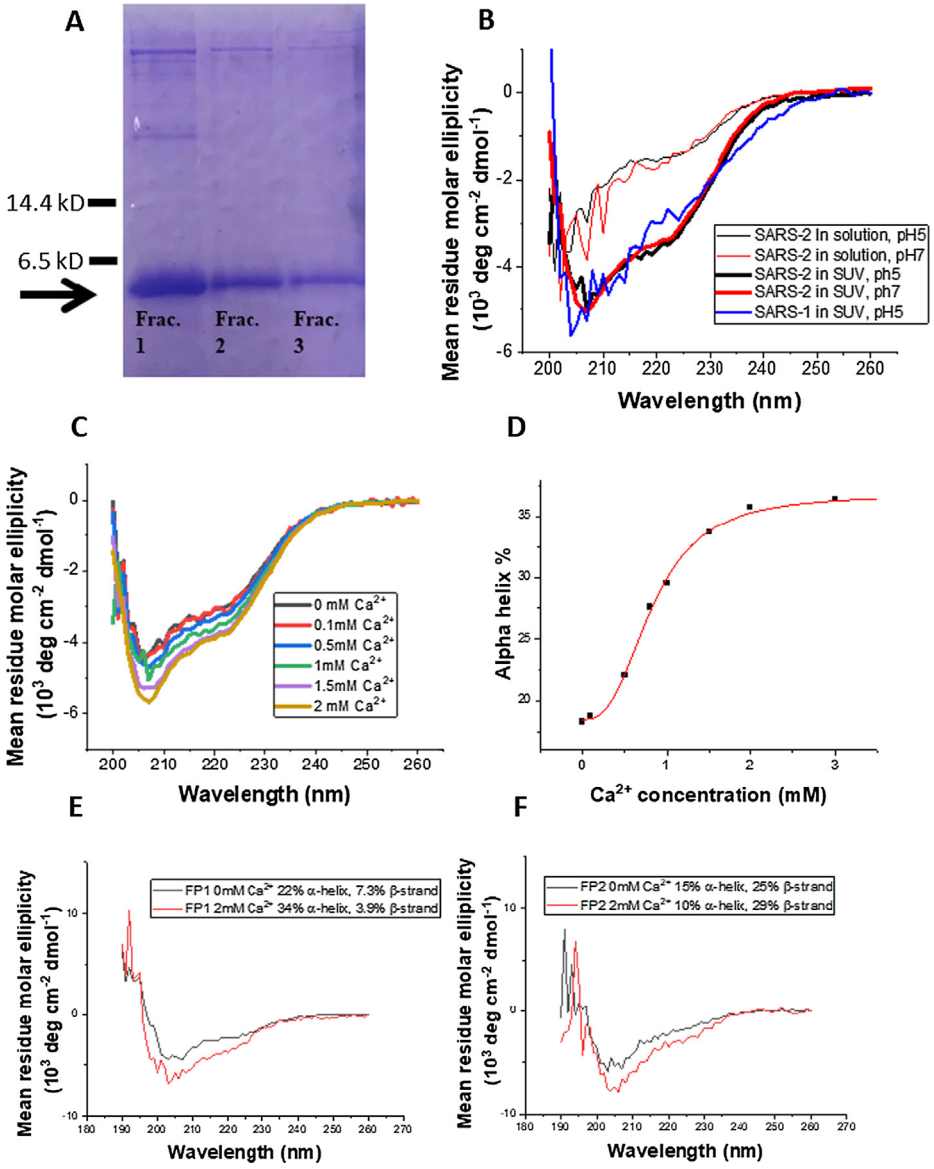


**Figure 2.** (A) The SDS-PAGE gel of the SARS-2 FP after purification using a His-tag affinity column; the arrow shows the bands for the FP. The fractions were the combined and further purified using size-exclusive chromatography. (B) CD Spectra of SARS-2 FP in solution (thin lines) and POPC/POPG/Chol = 3/1/1 SUVs (thick lines) in pH 5 buffer (black) or pH 7 buffer (red) at 25 °C, and SARS-1 FP in SUVs at pH5 (blue). (C) CD spectra for SARS-2 FP in SUVs at pH5 show that the alpha helix content increases with the increase of $Ca^{2+}$ concentration. (D) The alpha helix content of the FP in membranes at different $Ca^{2+}$ concentrations, which was calculated from (C) using K3D2 server.[54] The data were fit with the built-in logistic function of Origin, which shows the $X_{50}$ = 0.83 mM. (E, F) The CD spectra of SARS-2 FP1 (E) and FP2 (F) in SUV in pH5 buffer with 0 mM (black) and 2 mM (red) $CaCl_2$. The percentage of alpha helix and beta strand was calculated using K3D2.

vesicles (SUVs) composed of POPC/POPG/Chol = 3/1/1 and 1 mM $CaCl_2$ at pH 5. Here, we used SUVs instead of multilamellar lipid vesicles (MLVs) or large unilamellar vesicles (LUV) because MLVs and LUVs are too large for CD spectroscopy, since they would cause scattering and a noisy signal. We measured the CD spectra for SARS-1 FP under the same conditions, and found them similar to those of the SARS-2 FP, though the helical content of the SARS-2 FP is slightly greater in the membranes (27.6% for SARS-1, and 29.5% for SARS-2). To test the effect of pH on the secondary structure, we measured the CD spectra at pH5 and pH7. As shown in Figure 2B, the pH has little effect on the secondary structure of the SARS-2 FP in both the presence and absence of SUVs with 1 mM $Ca^{2+}$. The structure in membranes consists of 29% alpha helix and 7% beta strand. To test the effect of $Ca^{2+}$ on the secondary structure, we increased the $Ca^{2+}$

concentration from 0 to 3 mM, and we found that the alpha helical contents of the SARS-2 FP in the SUV at pH5 increases from 18% to 35%, saturating around 2 mM (cf. Figure 2C and D). To identify the source of helical increase, we synthesized separately the FP1 domain and the FP2 domain and repeated the CD experiments. As shown in Figure 2E and 2F, FP1 has a higher percentage of alpha helical structure than beta strand, while FP2 has the opposite. This result is consistent with the newly published structural model of SARS-2 FP using molecular dynamics[22] (and we adopted this MD model in Figure 1A). The presence of $Ca^{2+}$ promotes the formation of alpha helix in FP1 but promotes the formation of beta strand in FP2. Thus, the CD spectra show that the SARS-2 FP is affected by binding to SUV membranes and $Ca^{2+}$ has an overall effect of aiding the development of its secondary structure.

## SARS-2 FP increases membrane ordering

The ESR signal of the spin labels attached to the lipids in membrane bilayers is sensitive to the local environment. Four spin labels were used: DPPTC has a tempo-choline headgroup and the spin is sensitive to changes of environment at the headgroup region; 5PC, 10PC and 14PC have a doxyl group in the C5, C10 or C14 position respectively of the acyl chain (Figure 1B), and they are sensitive to the changes of local environment in the hydrophobic acyl chain region at the different depths. Using the NLSL software based on the MOMD model,[29,30] the order parameter of the spin can be extracted, which is a direct measure of the local ordering of the membrane. Thus, the effect of peptide binding on the structure of the membrane can be monitored. These four spin-labeled lipids have been used in previous studies, and their ability to detect changes in membrane structure has been validated.[21,31] Our previous studies examined the effect of various viral FPs, including those of influenza virus,[14,17] HIV,[16] Dengue Virus,[20] Ebolavirus (EBOV),[19] SARS-1,[18] and MERS,[24] as well as the FP of the ancestral eukaryotic gamete fusion protein HAP2.[20] All of these peptides were found to induce membrane ordering in the headgroup region as well as in the shallow hydrophobic region of bilayers (i.e., 5PC).

We used multilamellar vesicles (MLVs) in our ESR study as they can be much more concentrated than small unilamellar vesicles (SUVs) which greatly enhances the ESR signal. Furthermore, the use of MLVs is consistent with our previous studies.[16,17,20] As shown in Figure 3A, for the MLVs composed of POPC/POPG/Chol = 3/1/1, when the peptide:lipid ratio (P/L ratio) of FP increases from 0 to 5 mol%, the order parameter $S_0$ of DPPTC increases significantly from 0.44 to 0.49 at pH 5 and in the presence of 1 mM $Ca^{2+}$ (with the effect of varying the $Ca^{2+}$ concentration described in the next subsection). The increase of the $S_0$ is similar to the effect of the influenza FP as we have previously shown.[14–18,20,24] The membrane order of 5PC also significantly increases from 0.53 to 0.65 at pH 5 when the P/L ratio increases (Figure 3B). The perturbation of the FP to the lipid bilayers exists down to 10 PC, although the effect is not as large (from 0.32 to 0.35, Figure 3C). There is virtually no effect on the $S_0$ of 14PC (cf. Figure 3D). The pH seems not to have a substantial effect from a comparison of results at pH5 and pH7; however, acidification does boost the effect modestly (Figure 3E). To show that the ordering effect is sequence-specific, we synthesized a peptide that has the same residues as the SARS-2 FP but in a shuffled order as a control. As shown in Figure 3E, the shuffled-sequence peptide does not affect the membrane order at all. Clearly, the sequence of the FP is very important for its membrane ordering activity.

We also compared the effect of the SARS-2 FP to the SARS-1 FP and the MERS FP. As shown in Figure 3A and 3B, the shape of the S-curves of the SARS-2 and the SARS-1 FPs are similar in that they both saturate at around 2% P/L ratio, while the shape of the curve of the MERS FP is quite different in that it does not saturated even at 5% P/L ratio. It is worth mentioning that the 5% P/L ratio is very large in a natural scenario and that is why we did not increase the concentration further in our experiments. In an effort to quantify our results, we fit the $S_0$ vs P/L ratio curves for DPPTC (Figure 3A) and 5PC (Figure 3B) using the Hill equation $\Delta S_0 = \frac{\Delta S_{0,\min} - \Delta S_{0,\max}}{1+(X/X_{50})^p} + \Delta S_{0,\max}$ with fixed $S_{0,\min}$ and flexible $S_{0,\max}$, and also extracted the $X_{50}$ and p from the fittings. The $X_{50}$ represents the P/L ratio for the FP to reach its half maximum effect, and the p value might be viewed as the cooperativity of the peptide when it induces membrane ordering. We compare the Max $\Delta S_0$, $X_{50}$ and p values for the three CoV FP (Tables 1A and 1B, for DPPTC and 5PC respectively). We find that the maximal effect of the SARS-2 FP is greater than that of the SARS-FP (0.051 vs 0.039 for DPPTC and 0.12 vs 0.09 for 5PC) which is again greater than that of the MERS FP. The $X_{50}$ values of the SARS-2 and SARS-1 FPs are almost the same (0.26 and 0.29 for DPPTC and 0.23 and 0.22 for 5PC), and they are both significantly smaller than that of the MERS FP (0.60 and 1.14 for DPPTC and 5PC, respectively). The p values for the SARS-2 FP are smaller than those for the SARS-1 FP but greater than those for the MERS FP. In conclusion, the SARS-2 fusion peptide shows a greater membrane ordering effect than does the SARS-1 FP and the MERS FP.

## The SARS-2 FP-induced membrane ordering is calcium dependent

We have previously found that the EBOV,[19] SARS-1[18] and MERS[24] FPs perturb the membrane

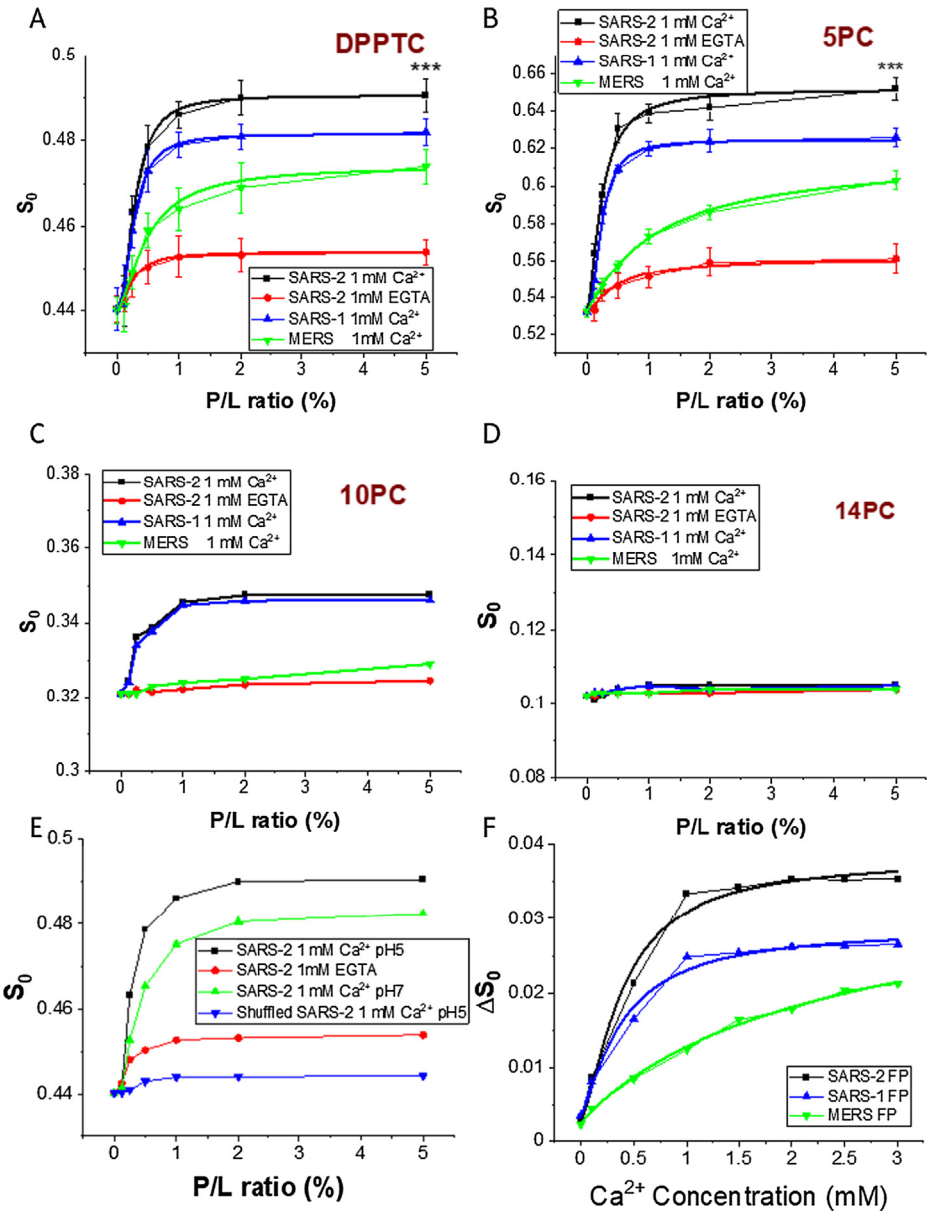


**Figure 3.** Plots of order parameters of DPPTC (A), 5PC (B), 10PC (C) and 14PC (D) versus peptide:lipid ratio (P/L ratio) of SARS-2 FP, SARS FP and MERS FP in POPC/POPG/Chol = 3/1/1 MLVs in buffer at pH5 with 150 mM NaCl at 25 °C. Black, SARS-2 FP with 1 mM $Ca^{2+}$ and at pH 5; red, SARS-2 FP with 1 mM EGTA; blue, SARS FP with 1 mM $Ca^{2+}$; green, MERS FP with 1 mM $Ca^{2+}$. The curves were fitted with the logistic function (Table 1A and 1B) (E). Plots of local order parameters of DPPTC versus P/L ratio as in A-D with pH indicated. Black, SARS-2 FP at pH 5; red, SARS-2 FP triple mutant (E4A_D5A_D15A) at pH 5; blue, SARS-2 FP at pH 7; and green, a peptide with shuffled sequence of SARS-2 FP at pH 5. (F) Plot of local order parameters of DPPTC with and without 1% peptide binding ($\Delta S_0$) versus $Ca^{2+}$ as in A-D. Black, SARS-2 FP; blue, SARS FP and green, MERS FP. The experiments were typically repeated three times. The typical uncertainties from simulation found for $S_0$ range from 1–5 $\times$ $10^{-3}$, while the uncertainties from repeated experiments were 5–8 $\times$ $10^{-3}$ or less than ± 0.01. We show in Panels A and B the bars for the standard deviation. Statistical significance analyses were performed using two-tailed Student's *t*-test on the $S_0'$s of 0% SARS-2 FP and 5% SARS-2 FP at the "1mM $Ca^{2+}$" condition, *** $\leq$ 0.001, highly significant.

structures in a $Ca^{2+}$ dependent fashion. Because of the similarity between the SARS-1 and SARS-2 FPs, we expected to observe this $Ca^{2+}$ dependency in the SARS-2 FP as well. For comparison we prepared a "calcium-free" buffer by not adding $Ca^{2+}$ and instead adding 1 mM of the chelating agent EGTA to further remove traces of $Ca^{2+}$. As shown in Figure 3A and B, the membrane ordering effects of the SARS-2 FP is suppressed. The small increase of $S_0$ when the P/L ratio increases, we call

Table 1 $S_0$ vs P/L ratio curve (Figure 3A and 3B), fitting with Hill equation $\Delta S_0 = \frac{\Delta S_{0,min} - \Delta S_{0,max}}{1+(X/X_{50})^p} + \Delta S_{0,max}$ with fixed $S_{0,min}$ and flexible $S_{0,max}$.

**(1A) DPPTC**

| | SARS-2 | SARS | MERS |
|---|---|---|---|
| Max ($\Delta S_0$) | 0.051 | 0.042 | 0.034 |
| $X_{50}$ (mM) | 0.26 | 0.29 | 0.52 |
| p | 2.16 | 2.32 | 1.54 |

**(1B) 5PC**

| | SARS-2 | SARS | MERS |
|---|---|---|---|
| Max ($\Delta S_0$) | 0.12 | 0.08 | 0.07 |
| $X_{50}$ (mM) | 0.23 | 0.23 | 1.09 |
| p | 1.67 | 2.13 | 1.06 |

"basal activity" for the SARS-2 FP, but this is insignificant compared to that in the presence of $Ca^{2+}$.

In order to further examine the effects of $Ca^{2+}$ on FP-inducing membrane ordering, we maintained the P/L ratio of the FP at a constant 1 mol%, and measured the order parameter $S_0$ with increasing calcium concentrations ranging from 0 to 3.0 mM (Figure 3F); the highest calcium concentration used here is much higher than the extracellular concentration of $Ca^{2+}$ in human adult lungs (ca. 1.3 mM).[32] The increase in $S_0$ affected by the presence of both the FPs and the $Ca^{2+}$; so, we generated a $\Delta S_0$-$Ca^{2+}$ concentration plot, where $\Delta S_0 = S_0$ (membrane with 1% FP) $- S_0$ (membrane without FP) vs. $Ca^{2+}$ concentration. This subtraction cancels any membrane ordering induced just by $Ca^{2+}$, with the $\Delta S_0$ at each $Ca^{2+}$ concentration representing only the contribution of $Ca^{2+}$ interacting with the FPs.

As shown in Figure 3F, $Ca^{2+}$ increases the $\Delta S_0$ of all three CoV FPs. However, while the response pattern to the $Ca^{2+}$ concentration is again similar within the SARS FPs, it is different from that of the MERS FP. We fit the $\Delta S_0$ vs $Ca^{2+}$ concentration curves with the Hill equation $\Delta S_0 = \frac{\Delta S_{0,min} - \Delta S_{0,max}}{1+(X/X_{50})^p} + \Delta S_{0,max}$ with fixed $\Delta S_{0,min}$ and flexible $\Delta S_{0,max}$ (Table 2), where $X_{50}$ is the $Ca^{2+}$ concentration that reaches 50% effectiveness, and the p value is the Hill slope interpreted as the cooperativity of the $Ca^{2+}$ binding to the FP. While the $X_{50}$ of the SARS-2 and SARS-1 FP are close (0.42 mM and 0.39 mM, respectively), the $X_{50}$ of the MERS FP is much larger (2.85 mM). The Hill slopes for SARS-2 and SARS FP are 1.67 and 1.30 respectively, indicating a positive cooperative binding of $Ca^{2+}$ to the FP, while the Hill slope for the MERS-FP (0.90) is appears not to be cooperative. We have shown previously that the SARS-1 FP binds two $Ca^{2+}$ ions, each on FP1 and FP2,[18] and the MERS FP binds only one $Ca^{2+}$ ion, possibly on FP1.[24] The difference between the Hill slopes appears to reflect this difference.

Table 2 $\Delta S_0$ vs $Ca^{2+}$ concentration curve (Figure 3F), fitting with Hill equation $\Delta S_0 = \frac{\Delta S_{0,min} - \Delta S_{0,max}}{1+(X/X_{50})^p} + \Delta S_{0,max}$ with fixed $\Delta S_{0,min}$ and flexible $\Delta S_{0,max}$.

| | SARS-2 | SARS | MERS |
|---|---|---|---|
| Max ($\Delta S_0$) | 0.032 | 0.023 | 0.018 |
| $X_{50}$ (mM) | 0.42 | 0.39 | 2.85 |
| p (Hill Slope) | 1.67 | 1.30 | 0.90 |

## Enthalpy changes of FP-membrane interactions

The importance of $Ca^{2+}$ can be further studied by comparing membrane binding enthalpies of FPs as measured by isothermal titration calorimetry (ITC) in the presence and absence of $Ca^{2+}$. In this experiment, small amounts of peptide were injected into a reaction cell containing a large excess of SUVs. Thus, during the whole titration process the amount of available membrane can be regarded as constant, and all injected peptides can be regarded as binding to the membranes. As a result, the reaction heat in each injection is equal. The enthalpy of reaction can be calculated from the average of heat in each injection.[33,34] We performed this experiment in the buffer with or without 1 mM $Ca^{2+}$. We then compared the difference in reaction enthalpy, which is caused by the presence of $Ca^{2+}$.

As shown in Table 3A, the binding enthalpy of the CoV-FPs is greater in the presence of $Ca^{2+}$ than in its absence. In both cases, the $\Delta H$ for SARS-2 and SARS-1 FP is greater than the MERS FP for this exothermic reaction with that for SARS-2 being significantly greater than for SARS-1 only in the presence of $Ca^{2+}$. When the difference between the with/without $Ca^{2+}$ cases was compared ($\Delta\Delta H \equiv \Delta H$ (in presence of $Ca^{2+}$) – $\Delta H$ (in absence of $Ca^{2+}$)), the $\Delta\Delta H$ of SARS-2 is greater than that of SARS-1 FP, which is greater than that for MERS FP. The enthalpy of FP-membrane binding mainly results from the folding of the FP.[35,36] Thus, the results suggest that: (1) SARS-2 FP folding is stronger than that of the SARS-1 FP and even more so than that of the MERS FP; (2) While $Ca^{2+}$ appears to promote the folding of the FP, it does it more effectively for the two SARS FPs than the MERS FP. That $Ca^{2+}$ promotes SARS-2 FP folding is consistent with the CD results (Figure 2C and 2D) which show the alpha helical content increases as the [$Ca^{2+}$ ] increases reaching a plateau for [$Ca^{2+}$] > 2 mM. This may be compared with the ESR observation that the $Ca^{2+}$ promotes FP-induced membrane ordering in a similar [$Ca^{2+}$] dependent manner (compare Figure 3A,B with Figure 2D).

## Interactions of FPs with calcium ions detected by ITC

We also used ITC to investigate whether $Ca^{2+}$ ions directly interact with SARS-2 FPs. During this

Table 3 Thermodynamic parameters measured using isothermal titration calorimetry.

A. Binding enthalpy of FPs to POPC:POPG:Chol = 60:20:20 SUVs at 37 °C at 1 mM $Ca^{2+}$ and at pH 5, obtained by titrating the FP into SUVs. The average and standard deviations were calculated from three repeats.

| Peptide | ΔH (kCal/mol) In 1 mM $Ca^{2+}$ | ΔH (kCal/mol) In 1 mM EGTA | Difference ΔΔH (kCal/mol) |
|---|---|---|---|
| SARS-2 FP | − 37.9 ± 0.4 | –32.3 ± 0.5 | 5.6 |
| SARS-1 FP | − 34.8 ± 0.4 | −31.8 ± 0.3 | 3.0 |
| MERS FP | − 26.4 ± 0.6 | −24.4 ± 0.4 | 2.0 |

B. Interaction between $Ca^{2+}$ cations and the FPs measured at 37 °C, obtained by titration the $Ca^{2+}$ into FP in solution. ΔH (reaction enthalpy), $K_b$ (binding constant), and n (stoichiometry) were calculated from the fitting using the one-site model. The average and standard deviations were calculated from three repeats.

| Peptides | ΔH (kCal/mol) | $K_b$ ($\times 10^4$ $M^{-1}$) | N | ΔG (kCal/mol) | -TΔS (kCal/mol) |
|---|---|---|---|---|---|
| SARS-2 | 7.2 ± 0.4 | 2.7 ± 0.2 | 1.86 ± 0.06 | 6.3 | −0.9 |
| SARS-2 _E4A_D5A_D15A | 5.5 ± 0.5 | 1.0 ± 0.2 | 1.03 ± 0.06 | 5.6 | 0.1 |
| SARS-1 | 6.8 ± 0.5 | 2.5 ± 0.3 | 1.70 ± 0.04 | 6.2 | −0.5 |
| MERS | 3.1 ± 0.4 | 1.1 ± 0.2 | 1.12 ± 0.08 | 5.6 | 2.5 |

titration, the $Ca^{2+}$ was titrated into the reaction cell with FPs in solution. Substantial heat absorbed during the titration was observed, with the heat absorbed saturating toward the end of the titration. As shown in Figure 4 and Table 3B, when the ΔH vs. $Ca^{2+}$:FP molar ratio plot was fitted using a one-site model, that makes the simple assumption that all binding sites have the same binding affinity, the enthalpy change is ΔH = 7.2 kCal/mol, with a binding constant $K_b = 2.7 \times 10^4$ $M^{-1}$ and stoichiometry n = 1.86. From these parameters, we further calculated the free energy change $\Delta G = -RT\ln K_b = 6.3$ kCal/mol and $-T\Delta S = \Delta G - \Delta H = -0.9$ kCal/mol. Thus, the calcium/SARS-2 FP interaction is endothermic, and the binding ratio is two calcium ions per peptide. The reason why the reaction is endothermic could be because the buffer solution (150 mM NaCl) contains large

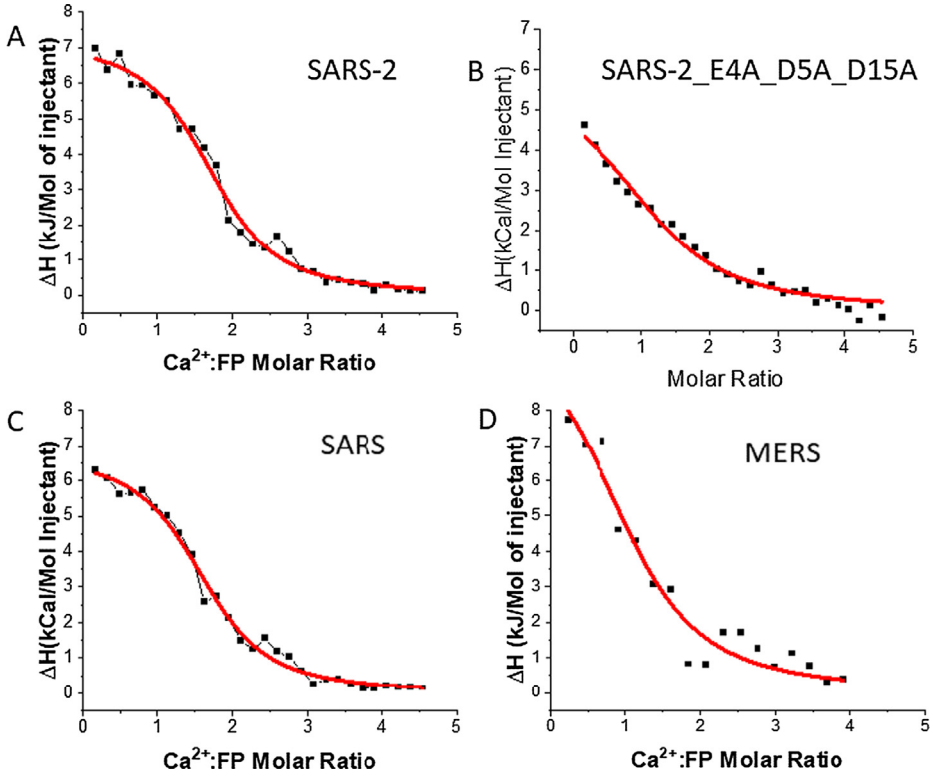


**Figure 4.** ITC analysis of $Ca^{2+}$ binding to FP of the coronaviruses. (A) SARS-2 FP, (B) SARS-2 FP triple mutant (E4A_D5A_D15A). (C) SARS-1 FP. (D) MERS FP. The peptides were titrated with $CaCl_2$ in the pH5 buffer. The integrated data represent the enthalpy change per mole of injectant, ΔH, in units of kcal/mol as a function of the molar ratio. The data were fitted using a one-site model (parameters shown in Table 3B). Data points and fitted data are overlaid.

amounts of $Na^+$ ions that could also interact with FP and that a stronger binding of $Ca^{2+}$ cations displaces bound $Na^+$ into the bulk solution. To test this hypothesis, we reduced the NaCl concentration to 50 mM and performed an ITC titration. However, the baselines of the titration curve we obtained were unstable, and we could not extract meaningful data. The reason for this result is unclear, but it is likely that the peptide requires a certain level of salt concentration to maintain its structure.

We performed the same experiment with the SARS-1 FP and the MERS FP (Figure 4C and 4D). As shown in Table 3B, like SARS-2 FP, SARS-1 FP also exhibits an endothermic reaction with $Ca^{2+}$, with a stoichiometry of n = 1.70, $\Delta H$ = 6.8 kCal/mol, and $K_b = 2.5 \times 10^4\ M^{-1}$. For the MERS FP, the stoichiometry is n = 1.12, suggesting that it only binds one $Ca^{2+}$, and the $\Delta H$ (3.1 kCal/mol) is significantly lower than that of the SARS-1 FPs, also resulting from the less $Ca^{2+}$ binding. We also generated a triple mutation on the SARS-2 FP (E4A_D5A_D15A), which completely removed the potential $Ca^{2+}$ binding site on the FP1 section. As shown in Figure 4B and Table 3B, the n is reduced to 1.03, which is coincident with our hypothesis that the triple mutant can only bind one $Ca^{2+}$ ion in its FP2 section. In conclusion, these ITC experiments demonstrate strong evidence for direct calcium-FP interactions, and we associate it with one $Ca^{2+}$ cation binding per FP1 or FP2.

## The $Ca^{2+}$ dependency is highly specific

We have already shown that the SARS-2 FP induces membrane ordering in a $Ca^{2+}$ dependent fashion. But how specific is it? In order to address this question, we have repeated the ESR experiment in the presence of a number of different ions, including most of the biologically relevant ions ($Mg^{2+}$, $Al^{3+}$, $K^+$, $Fe^{2+}$, $Fe^{3+}$, $Zn^{2+}$, $Mn^{2+}$) as well as $Tb^{3+}$ which is not biologically relevant but is widely used as a $Ca^{2+}$ substitute as its size is similar to $Ca^{2+}$.[37] We used the 1 mM EGTA case as a control; as mentioned above even without any $Ca^{2+}$, the FP has a "basal" activity. We did not measure the effect of $Na^+$ as there is 150 mM $Na^+$ in the buffer, which provides the necessary ionic strength for the folding of the FP. As shown in Figure 5A, the membrane ordering activity of the FP in the presence of all other ions except $Tb^{3+}$ is significantly lower than that in the presence of $Ca^{2+}$. The $Tb^{3+}$ case is the closest to the $Ca^{2+}$ case, but still substantially smaller. The $K^+$ has almost zero effect on the activity; it is almost the

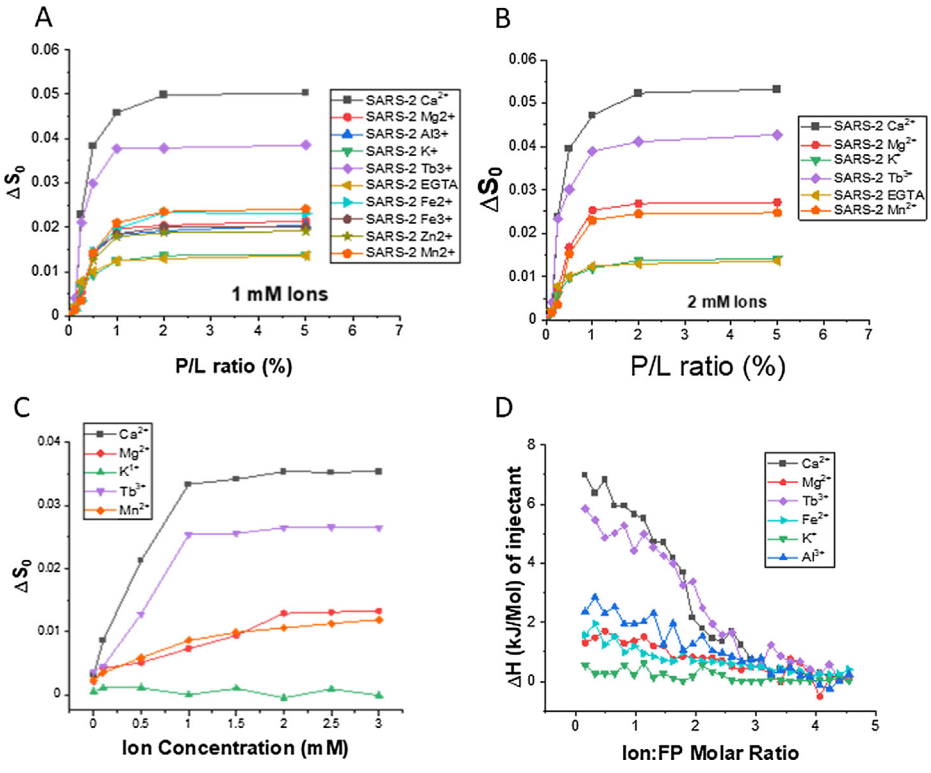


**Figure 5.** The specificity of $Ca^{2+}$. (A) Plots of local order parameter changes of DPPTC ($\Delta S_0$) versus the P/L ratio with 1 mM ion concentration for a variety of ions and in buffer with 150 mM NaCl at pH5 and at 25 °C. (B) The same with 2 mM ion concentration. (C) Plots of local order parameter changes of DPPTC ($\Delta S_0$) versus the concentration of the ions with 1% P/L ratio and at pH5. (D) ITC analysis of ions binding to SARS-2 FP in solution. The peptides were titrated with $CaCl_2$ in pH5 buffer.

same as the EGTA case. When the concentration of some ions increases to 2 mM (Figure 5B), the trends are the same. We then fixed the P/L ratio to 1% and increased the concentration of ions (Figure 5C), we again find that the $Ca^{2+}$ and $Tb^{3+}$ will allow the FP to function more effectively (as measured by $\Delta S_0$) in higher concentrations, while the $Mg^{2+}$ and $Mn^{2+}$ only boost the effect slightly. We repeated the ion-FP ITC experiments for several ions, and one sees from Figure 5D, that while the $Tb^{3+}$ curve is comparable to that of the $Ca^{2+}$, the other ions have a significantly lower reaction heat than the $Ca^{2+}$, which again shows the specificity of $Ca^{2+}$-FP binding.

## Discussion

The mechanism of membrane fusion is still only partially understood. Our past work has shown that numerous viral FPs induce increased membrane ordering in a collective fashion, i.e., a significant increase in $S_0$ as a function of the P/L ratio.[14,15,17–20,24,38] We further suggested that FP-induced membrane ordering is accompanied with dehydration resulting from peptide insertion, and this is a prerequisite step for removal of the repulsive forces between two opposing membranes, thereby facilitating initialization of membrane fusion.[14–17,20] We, in conjunction with our collaborators, have also determined that the CoVs (SARS-1, SARS-2, and MERS) and EBOV requires $Ca^{2+}$ for viral entry and that the $Ca^{2+}$ binding site is on the FP.[18,19] Our current study extends these observations to the SARS-2 FP revealing several new features.

We have established the hypothesis[25] that the sequence immediately downstream from the S2′ cleavage site is the *bona fide* SARS-1 FP.[18] Thus, we predicted that the homologous sequence on the SARS-2 S protein to the SARS-1 FP is also the *bona fide* SARS-2 FP. We have now shown that this SARS-2 FP does effectively induce membrane ordering, thereby confirming it must be the FP for the SARS-2 S protein. We also showed that it perturbs the membrane structure in a $Ca^{2+}$ dependent fashion as do the SARS-1 and MERS FPs.

Although this result was expected considering the similarity between SARS-2 and SARS-1 FPs, we did find that SARS-2 FP leads to greater membrane ordering than SARS-1 FP, especially in the head group and upper hydrophobic regions. It both induces a greater degree of membrane ordering and has smaller $X_{50}$ values. The SARS-2 FP also has a greater level of response to the $Ca^{2+}$ concentration (cf. Figure 3F and Table 2) as it has a greater Max($\Delta S_0$) and the Hill slope is greater. This is supported by the fact that the SARS-2 FP has a higher binding enthalpy than the SARS-1 FP (cf. Table 3A). All the above suggest that the SARS-2 FP is more effective in membrane binding and $Ca^{2+}$ binding than SARS-1 FP.

Since there is only a three residue difference between the SARS-2 and SARS-1 FPs, the most reasonable cause for the difference between the activity of these two FPs must be in these three residues. We suspect that the greater hydrophobicity of the three residues in SARS-2 FP is the cause. The hydropathy index for Ile (4.5), $Asp^{-}$ (−3.5) and Ala (1.8) of the SARS-2 FP is greater than or equal their counterparts (Met (1.9), $Glu^{-}$ (−3.5) and Gln (−3.5)) of the SARS-1 FP (a greater positive value means more hydrophobic).[39] Thus, the grand average of hydropathy value (GRAVY) for SARS-2 FP is also greater than the SARS-1 FP (cf. Figure 1C). In the case of peptide-membrane interaction, the interface scale of hydrophobicity is more useful as it measures the free energies of transfer $\Delta G$ (kCal/mol) from water to POPC interface.[40] The interface scale of the Ile (-0.31), $Asp^{-}$ (1.23) and Ala (0.17) of the SARS-2 FP is also greater than their counterparts (Met (-0.23), $Glu^{-}$(2.02), and Gln (0.58)) of the SARS-1 FP[40] (here more negative value means more hydrophobic), thus the overall interface scale value for the SARS-2 FP is also significantly more hydrophobic than the SARS-1 FP.

In the process of the FP interacting with the membrane, most of the driving force comes from the enthalpy gain by the folding of FP, whereas the opposing force comes from the entropy loss of restricting the FP on the membrane surface.[27,35,36] The latter can be partly compensated by releasing water molecules during a hydrophobic interaction between the FP and the hydrophobic region of the membrane. The more hydrophobic SARS-2 FP interacts with the hydrophobic core more strongly, inserts more deeply into the membrane, and likely releases more water molecules in the headgroup region, thus reducing the entropy loss more effectively than does the SARS-1 FP. The SARS-2 FP also has a greater effect on the shallower hydrophobic region (5PC, Figure 3B). The folding of the FP is also modulated by how deep it inserts into the membrane. We observed that the enthalpy release of the SARS-2 FP-membrane insertion is greater, indicating better folding than the SARS-1 FP in the membrane, which also increases the driving force of the FP-membrane interaction.

These mutations also account for the better $Ca^{2+}$-FP binding and the better $Ca^{2+}$ response of the SARS-2 FP. Asp has been shown to have a greater $Ca^{2+}$ binding affinity than Glu in aqueous solution.[41] Although Ala may not directly be involved in the interaction with $Ca^{2+}$ in this case, it has a greater $Ca^{2+}$ affinity than Gln even at high pH.[42]

The greater ordering effect of the SARS-2 FP implies that SARS-2 enters the host cells more effectively than SARS-1 in the initiation stage of membrane fusion. As membrane fusion is a required step in the infection by the CoV and the initiation stage (i.e., membrane ordering) is a

required stage in membrane fusion, it suggests that this may be one of the reasons why the SARS-2-CoV invades host cells more easily. The greater [$Ca^{2+}$] response also implies that control of its access to $Ca^{2+}$ could reduce its infectivity.

By comparing the two SARS FPs and the MERS FP, we found that the MERS FP is less effective than the SARS FPs (i.e., less $S_0$ increase at the same P/L ratio) and its $Ca^{2+}$-dependence is also less responsive (i.e., the enhancement of $S_0$ by the MERS FP is less at the same $Ca^{2+}$ concentration than that of the SARS FPs, and it only binds one $Ca^{2+}$ ion while the SARS FPs binds two). However, MERS still appears to be a "successful" virus. It raises an interesting question why MERS is still successful when its FP is less effective than the SARS FPs. There may be several reasons. First, MERS-CoV is a less lethal virus compared to the SARS-CoVs, which gives it an advantage in transmission. Second, the infectivity of virus depends on other factors such as the binding to surface receptors, the activation by protease cleavage, gene replication, assembly of virion particle and budding, etc. It is possible MERS does better in the other aspects. Third, the membrane fusion during viral entry can occur either on the cell plasma membrane surface or in the endosome.[43,44]. While the two SARS-CoVs are known to enter cells mainly through the endocytic pathway,[43] MERS can enter the host cells via both pathways.[24] As the plasma membrane pathway is not $Ca^{2+}$ dependent, the entry of MERS is less $Ca^{2+}$ dependent as a whole. Finally, we cannot exclude the possibility that other segments on S2 would also play a role in the membrane fusion. We have confirmed previously[18] in the SARS-1 case that the sequence immediately downstream of the S2' (aka. FP1_2) is the *bona fide* fusion peptide by comparing the membrane ordering effect of the FP to the other two potential candidates (the sequence in the downstream of S1/S2 cleavage site (770–788), and the "internal" peptide (873–888), AltFP-A and AltFP-B respectively as we referred to in that paper). However, it remains to be clarified whether these two peptides play an assisting role, that is they may further help to increase the membrane ordering. In the SARS-2 case (Wuhan-Hu-1 strain, NCBI Reference Sequence: NC_045512.2, GeneID:43740568), the sequence of the homologous AltFP-B region is the same (891–906, GAALQIPFAMQMAYRF) as SARS-1, while the homologous AltFP-A region has several amino acids difference (788–806, *I*YKTP*P*I*K*DFGGFNFSQIL, the italic letters indicates the different residues). However, the homologous sequence for AltFP-B in the S protein of MERS-CoV (NCBI Reference Sequence: NC_019843.3, GeneID:14254594) is very different. And there is no homologous sequence to AltFP-A. Therefore, whether the "MERS AltFP-B" plays a role in membrane fusion and whether there is a sequence between the S1/S2 and S2' sites (corresponding to but not homologous to the AltFP-A in SARS-1 and SARS-2) plays a role are still unknown and worthy of clarification. It is possible that they have a more active role than the AltFP-A and AltFP-B in SARS-1 (and perhaps than those in SARS-2 as well), and thus "compensate" for the relatively lower membrane ordering activity of the MERS FP.

We further investigated how specific is the role of $Ca^{2+}$ in the activity of the SARS-2 FP. By comparing a series of ions, we found that the FP-$Ca^{2+}$ interaction is very specific. Although most other ions can enhance the membrane ordering slightly above the "basal activity," their effect is much smaller than that of the $Ca^{2+}$. The ion-FP interaction is also weaker, as revealed by ITC. Although the FP has negatively charged residues and should attract cations, this selectivity is likely to be governed by the many-body polarization effect,[45] which is an energetic cost arising from the dense packing of multiple residues around the metal ion. The many-body effect depends on the size of the ion, as well as the number and spatial arrangement of the residues around it. There are three negatively charged residues in either the FP1 or FP2 region which satisfies the requirement for a multi-body interaction. We also showed that the only close alternative candidate to $Ca^{2+}$ is $Tb^{3+}$, which has a size that is similar to that of $Ca^{2+}$ (radius of $Ca^{2+}$ and $Tb^{3+}$ in solution is 103 and 101 picometer respectively). We found the ion-FP interaction is endothermal. We suspect that the substantial amount of $Na^+$ already in solution initially interacts with the charged residues, and there is a more effective replacement by $Ca^{2+}$ during the titration. That is, ions with suitable size can efficiently replace the $Na^+$, but this suggestion requires verification.

Calcium ions play important roles in membrane fusion. In the case of cellular SNARE-mediated synaptic vesicle fusion, calcium ions directly interact with fusion protein machineries and have a role as activators for such fusion machinery.[46–48] But in contrast to the SNARE-mediated case, calcium plays the role of a modulator in the case of viral fusion. It enhances the fusion in two ways. Indirectly, because of its positive charges, calcium possesses a generally enhancing but indirect effect on membrane fusion by electrostatic interactions with negatively charged headgroups of the lipid bilayers and thus decreases the electrostatic repulsion of the two opposing membranes that are in close proximity prior to undergoing fusion. Also, calcium directly interacts with the FP of the fusogens and enhances their fusogenicity.

There are relatively few cases for which calcium plays such a direct role in viral membrane fusion, especially for an N-terminal FP. In the case of influenza and HIV with an N-terminal FP, calcium plays only an indirect enhancing effect on membrane fusion by affecting the membrane

only.[49] However, in cases such as CoVs, calcium also plays a direct role by interacting with the FP directly. Rubella infection has been shown to require $Ca^{2+}$, but its E1 envelope glycoprotein is a class II viral fusion protein that has an internal FP.[50] We have shown that the EBOV GP protein is another case for $Ca^{2+}$ dependence, but EBOV FP is an internal one.[19] In this study and our previous study,[18,24] we showed that the viral entry of members of the CoV virus family (SARS-1, SARS-2 and MERS), which all have an N-terminal FP (though whether other segments also play a role needs to be clarified as discussed above), are also $Ca^{2+}$ dependent.

Insights into the $Ca^{2+}$ dependency of the FP would help us to better understand the mechanism of SARS-2 infection, and should also help to determine whether the membrane fusion of SARS-2 occurs on the cell surface or inside the endosome by controlling the exocellular or intracellular [$Ca^{2+}$]. This could lead to therapeutic solutions that either target the FP-calcium interaction, or block the $Ca^{2+}$ channel, and also repurpose already approved drugs for the ongoing COVID19 pandemic.

## Materials and methods

### Lipids and peptides

The lipids POPC, POPG, and the chain spin labels 5PC, 10PC and 14PC and the head group spin label dipalmitoylphospatidyl-tempo-choline (DPPTC) were purchased from Avanti Polar Lipids (Alabaster, AL) or synthesized in our laboratory according to previous protocols. Cholesterol was purchased from Sigma (St. Louis, MO). The shuffled sequence of SARS-2 was generated using Sequence Manipulation Suite (http://www.bioinformatics.org/sms2/shuffle_protein.html), and this peptide was synthesized by Biomatik. The sequences of the peptides and the structure of the spin labeled lipids are shown in Figure 1C.

We previously cloned the SARS-1 FP gene into a pET31 expression vector, and the SARS-2 FP gene is generated by the point-mutagenesis from the SARS-1 FP clone. The mutations were generated using a USB Change-IT site directed mutagenesis kit (Affymetrix). The sequence has been confirmed in the sequencing service provided by the Biotechnology Core Facility (BRC) at Cornell University. The protocol of expression and purification also follows published procedures.[19,26] Briefly, the relevant plasmids were transformed in BL21(DE3) *Escherichia coli* competent cells and grown at 37 °C to an optical density ~0.8. Protein expression was induced for 3 hours at 30 °C by 0.5 mM IPTG. The harvested cells were lysed by sonication and clarified by centrifugation at 40,000 rpm for 45 minutes. The supernatant containing the His-tagged fusion protein was transferred to a pre-equilibrated Ni-NTA agarose resin column, and the supernatant and resin were incubated for 2 hours at 4 °C on a rotator in wash buffer (containing 25 mM Tris, 500 mM NaCl, 20 mM Imidazole, 5% glycerol, 5 mM β-ME, and 10 mM CHAPS, pH 8). The resin was then rinsed with digestion buffer (containing 25 mM Tris, 50 mM NaCl, 5 mM CaCl2, and 5% glycerol, pH 7.5). 125 μL of Factor Xa (1 mg/mL) in 15 mL digestion buffer was added to the resin and incubated overnight at room temperature. The proteins were eluted using 50 mL wash buffer, dialyzed against dialysis buffer (25 mM Tris, 50 mM NaCl, 5% Glycerol, pH 8.5), and purified using a Superdex Peptide 10/300 GL gel-filtration column (GE Healthcare). The yield of the FP is approximately 0.8 mg/L. The scrambled FP, FP1, and FP2 were purchased from BioMatik (Wilmington, DE).

### Vesicle preparation

The composition of membranes used in this study is consistent with our previous study.[25] The desired amounts of POPC, POPG, cholesterol and 0.5% (mol:mol) spin-labeled lipids in chloroform were mixed well and dried by $N_2$ flow. The mixture was evacuated in a vacuum drier overnight to remove any trace of chloroform. To prepare MLVs, the lipids were resuspended and fully hydrated using 1 mL of pH 7 or pH 5 buffer (5 mM HEPES, 10 mM MES, 150 mM NaCl, and 0.1 mM EDTA, pH 7 or pH 5) at room temperature (RT) for 2 hours. To prepare SUVs for CD and ITC measurements and the PP-SUV system, the lipids were resuspended in pH 7 or pH 5 buffer and sonicated in an ice bath for 20 minutes or when the suspension became clear. The SUVs solution was then further clarified by ultracentrifugation at 13,000 rpm for 10 min.

### Circular dichroism (CD) spectroscopy

The CD experiments were carried out on an AVIV CD spectrometer Aviv Model 215. The peptides were mixed with SUVs in 1% P/L ratio with a final peptide concentration of 0.1 mg/mL at RT for more than 10 min before the measurements. The measurements were performed at 25 °C and two repetitions were collected. Blanks were subtracted and the resulting spectra were analyzed. The mean residue weight ellipticity was calculated using the formula: $[\Theta] = \theta/(10 \times c \times l \times n)$, where $\theta$ is the ellipticity observed (in degrees); c is the peptide concentration (in dmol); l is the path length (0.1 cm); and n is the number of amino acids per peptide.[34]

### Isothermal titration calorimetry (ITC)

ITC experiments were performed in an N-ITC III calorimeter (TA Instrument, New Castle, DE). To measure the enthalpy of FP membrane binding, FP at 20 μM was injected into 1 mL 5 mM SUV solution at 37 °C. Each addition was 10 μL, each

injection time was 15 sec, and each interval time was 5 min. Each experiment comprised about 25 to 30 injections. The data were analyzed with Origin (OriginLab Corp., Northampton, MA).

To measure the peptide-$Ca^{2+}$ interaction a total of 300 μL 2 mM $CaCl_2$ in pH 5 buffer was injected into 0.4 mM FP in pH 5 buffer at 37 °C in a stepwise manner consisting of 10 μL per injection except that the first injection was 2 μL. The injection time was 15 sec for each injection and the interval time was 10 min. The background caused by the dilution of $CaCl_2$ was subtracted by using data from a control experiment that titrated $CaCl_2$ in a pH 5 buffer. The data were analyzed with Origin. The one-site model was used in the fitting to calculate the thermodynamic parameters. The protein concentration is determined by dry weight and UV spectroscopy at wavelength = 280 nm with extinction coefficient $\varepsilon$ = 1520 $M^{-1}$ $cm^{-1}$ for SARS-2 and SARS-1 FP, and 4080 $M^{-1}$ $cm^{-1}$ for MERS FP in the oxidized condition.

### ESR spectroscopy and nonlinear least-squares fit of ESR spectra

To prepare the samples for lipid ESR study, the desired amounts of FPs (1 mg/mL) were added into the lipid MLVs dispersion. After 20 min of incubation, the dispersion was spun at 13,000 rpm for 10 min. The concentrations of peptide were measured using UV to ensure complete binding of peptide. The pellet was transferred to a quartz capillary tube for ESR measurement. ESR spectra were collected on an ELEXSYS ESR spectrometer (Bruker Instruments, Billerica, MA) at X-band (9.5 GHz) at 25 °C using a $N_2$ Temperature Controller (Bruker Instruments, Billerica, MA).

The ESR spectra from the labeled lipids were analyzed using the NLLS fitting program based on the stochastic Liouville equation[30,51] using the MOMD or Microscopic Order Macroscopic Disorder model as in previous studies.[14–17,20] The fitting strategy is described below. We employed the Budil *et al.* NLLS fitting program[30] to obtain convergence to optimum parameters. The g-tensor and A-tensor parameters used in the simulations were determined from rigid limit spectra.[14] In the simulation, we required a good fit with a small value of $\chi^2$ and also good agreement between the details of the final simulation and the experimental spectrum. Each experiment (and subsequent fit) was repeated 2 or 3 times to check reproducibility and estimate experimental uncertainty. Two sets of parameters that characterize the rotational diffusion of the nitroxide radical moiety in spin labels were generated. The first set is the rotational diffusion constants. $R_\perp$ and $R_\parallel$ are respectively the rates of rotation of the nitroxide moiety around a molecular axis perpendicular and parallel to the preferential orienting axis of the acyl chain. The second set consists of the ordering tensor parameters, $S_0$ and $S_2$, which are defined as follows: $S_0=<D_{2,00}>=<1/2(3\cos2\theta - 1)>$, and $S_2=<D^{2+}_{2,0}D_{2,0\text{-}2}> =<\sqrt{(3/2)}\sin2\theta\cos2\varphi>$, where $D_{2,00}$, $D_{2,02}$, and $D_{2,0\text{-}2}$ are the Wigner rotation matrix elements and $\theta$ and $\varphi$ are the polar and azimuthal angles for the orientation of the rotating axes of the nitroxide bonded to the lipid relative to the director of the bilayer, i.e., the preferential orientation of lipid molecules; the angular brackets imply ensemble averaging. $S_0$ and its uncertainty were then calculated in standard fashion from its definition and the dimensionless ordering potentials $C_{20}$ and $C_{22}$ and their uncertainties found in the fitting. The typical uncertainties we find for $S_0$ range from 1–5 $\times$ $10^{-3}$, while the uncertainties from repeated experiments are 5–8 $\times$ $10^{-3}$ or less than ± 0.01. $S_0$ indicates how strongly the chain segment to which the nitroxide is attached is aligned along the normal to the lipid bilayer, which is believed to be strongly correlated with hydration/dehydration of the lipid bilayers. As previously described, $S_0$ is the main parameter for such studies.[17,52,53]

## CRediT authorship contribution statement

**Alex L. Lai:** Investigation, Validation, Formal analysis, Data curation, Conceptualization, Methodology, Visualization. **Jack H. Freed:** Supervision, Resources, Conceptualization, Methodology, Visualization.

## Acknowledgement

This work was funded by NIH grants R01GM123779 and P41GM103521. We thank Dr. Susan Daniel and Dr. Gary Whittaker for providing numerous helpful discussions and suggestions. We also thank Dr. Harel Weinstein and Dr. George Khelashvili for sharing the results of their molecular dynamics study.

## Declaration of Competing Interest

The authors declare that they have no known competing financial interests or personal relationships that could have appeared to influence the work reported in this paper.

*Received 30 December 2020;*
*Accepted 11 March 2021;*
*Available online 18 March 2021*

***Keywords***:
COVID-19;
ESR;
ITC;
hydrophobicity;
ion specificity

***Abbreviations***:
CD, circular dichroism; CoV, coronavirus; ESR, electron spin resonance; FP, fusion peptide; ITC, isothermal calorimetry; LUV, large unilamellar vesicle; MERS, Middle East Respiratory Syndrome; MLV, multilamellar vesicle; MOMD, microscopic order but macroscopic disorder; POPC, 1-palmitoyl-2-oleoyl-glycero-3-phosphocholine; POPG, 1-palmitoyl-2-oleoyl-sn-glycero-3-phospho-(1′-rac-glycerol); SARS, Severe Acute Respiratory Syndrome; SUV, small unilamellar vesicle; TMD, transmembrane domain

## References


1. De Wit, E., Van Doremalen, N., Falzarano, D., Munster, V. J., (2016). SARS and MERS: Recent insights into emerging coronaviruses. *Nat. Rev. Microbiol.*, **14**, 523–534.
2. Epand, R.M., (2000). Membrane fusion. *Biosci. Rep.*, **20**, 435–441.
3. Blumenthal, R., Clague, M.J., Durell, S.R., Epand, R.M., (2003). Membrane fusion. *Chem. Rev.*, **103**, 53–69.
4. Weissenhorn, W. et al, (1999). Structural basis for membrane fusion by enveloped viruses. *Mol. Membr. Biol.*, **16**, 3–9.
5. Tang, T., Bidon, M., Jaimes, J.A., Whittaker, G.R., Daniel, S., (2020). Coronavirus membrane fusion mechanism offers a potential target for antiviral development. *Antiviral Res.*, **178**, 104792
6. Gui, M. et al, (2017). Cryo-electron microscopy structures of the SARS-CoV spike glycoprotein reveal a prerequisite conformational state for receptor binding. *Cell Res.*, **27**, 119–129.
7. Walls, A.C. et al, (2020). Structure, function, and antigenicity of the SARS-CoV-2 spike glycoprotein. *Cell*, **181**, 281–292.e6.
8. Wrapp, D. et al, (2020). Cryo-EM structure of the 2019-nCoV spike in the prefusion conformation. *Science (80- .)*,. https://doi.org/10.1126/science.aax0902.
9. Xia, S. et al, (2020). Inhibition of SARS-CoV-2 (previously 2019-nCoV) infection by a highly potent pan-coronavirus fusion inhibitor targeting its spike protein that harbors a high capacity to mediate membrane fusion. *Cell Res.*, **30**, 343–355.
10. Wang, Q. et al, (2020). Structural and functional basis of SARS-CoV-2 entry by using human ACE2. *Cell*,. https://doi.org/10.1016/j.cell.2020.03.045.
11. Georgieva, E.R., Ramlall, T.F., Borbat, P.P., Freed, J.H., Eliezer, D., (2010). The lipid-binding domain of wild type and mutant α-synuclein: Compactness and interconversion between the broken and extended helix forms. *J. Biol. Chem.*, **285**, 28261–28274.
12. Georgieva, E.R., Xiao, S., Borbat, P.P., Freed, J.H., Eliezer, D., (2014). Tau binds to lipid membrane surfaces via short amphipathic helices located in its microtubule-binding repeats. *Biophys. J.*, **107**, 1441–1452.
13. Snead, D. et al, (2017). Unique structural features of membrane-bound C-terminal domain motifs modulate complexin inhibitory function. *Front. Mol. Neurosci.*, **10**, 1–17.
14. Ge, M., Freed, J.H., (2009). Fusion peptide from influenza hemagglutinin increases membrane surface order: an electron-spin resonance study. *Biophys. J.*, **96**, 4925–4934.
15. Ge, M., Freed, J.H., (2011). Two conserved residues are important for inducing highly ordered membrane domains by the transmembrane domain of influenza hemagglutinin. *Biophys. J.*, **100**, 90–97.
16. Lai, A.L., Freed, J.H., (2014). HIV gp41 fusion peptide increases membrane ordering in a cholesterol-dependent fashion. *Biophys. J.*, **106**, 172–181.
17. Lai, A.L., Freed, J.H., (2015). Interaction between the influenza HA fusion peptide and transmembrane domain affects membrane structure. *Biophys. J.*, **109**, 1–14.
18. Lai, A.L., Millet, J.K., Daniel, S., Freed, J.H., Whittaker, G. R., (2017). The SARS-CoV fusion peptide forms an extended bipartite fusion platform that perturbs membrane order in a calcium-dependent manner. *J. Mol. Biol.*, **429**, 3875–3892.
19. Nathan, L. et al, (2020). Calcium ions directly interact with the ebola virus fusion peptide to promote structure-function changes that enhance infection. *ACS Infect. Dis.*, **6**, 250–260.
20. Pinello, J.F. et al, (2017). Structure-function studies link class II viral fusogens with the ancestral gamete fusion protein HAP2. *Curr. Biol.*, **27**, 651–660.
21. Ge, M., Freed, J.H., (2003). Hydration, structure, and molecular interactions in the headgroup region of dioleoylphosphatidylcholine bilayers: an electron spin resonance study. *Biophys. J.*, **85**, 4023–4040.
22. Khelashvili, G., Plante, A., Doktorova, M., Weinstein, H., (2021). Ca2+-dependent mechanism of membrane insertion and destabilization by the SARS-CoV-2 fusion peptide. *Biophys. J.*, **120**, 1105–1119.
23. Gautier, R., Douguet, D., Antonny, B., Drin, G., (2008). HELIQUEST: A web server to screen sequences with specific α-helical properties. *Bioinformatics*,. https://doi.org/10.1093/bioinformatics/btn392.
24. Straus, M.R. et al, (2020). Ca 2+ ions promote fusion of Middle East respiratory syndrome coronavirus with host cells and increase infectivity. *J. Virol.*, **94**, e00426–20.
25. Madu, I.G., Roth, S.L., Belouzard, S., Whittaker, G.R., (2009). Characterization of a highly conserved domain within the severe acute respiratory syndrome coronavirus spike protein S2 domain with characteristics of a viral fusion peptide. *J. Virol.*, **83**, 7411–7421.
26. Gregory, S.M. et al, (2011). Structure and function of the complete internal fusion loop from Ebolavirus glycoprotein 2. *Proc. Natl. Acad. Sci. U. S. A.*, **108**, 11211–11216.
27. Lai, A.L., Tamm, L.K., (2007). Locking the kink in the influenza hemagglutinin fusion domain structure. *J. Biol. Chem.*, **282**, 23946–23956.
28. Yao, H., Hong, M., (2014). Conformation and lipid interaction of the fusion peptide of the paramyxovirus PIV5 in anionic and negative-curvature membranes from solid-state NMR. *J. Am. Chem. Soc.*,. https://doi.org/10.1021/ja4121956.
29. Ge, M., Budil, D.E., Freed, J.H., (1994). An electron spin resonance study of interactions between phosphatidylcholine and phosphatidylserine in oriented membranes. *Biophys. J.*, **66**, 1515–1521.
30. Budil, D.E., Lee, S., Saxena, S., Freed, J.H., (1996). Nonlinear-least-squares analysis of slow-motion EPR spectra in one and two dimensions using a modified Levenberg-Marquardt algorithm. *J. Magn. Reson., Ser. A*, **120**, 155–189.

31. Lou, Y., Ge, M., Freed, J., (2001). A multifrequency ESR study of the complex dynamics of membranes. *J. Phys. Chem. B*, **105**, 11053–11056.
32. Brennan, S.C. et al, (2016). The extracellular calcium-sensing receptor regulates human fetal lung development via CFTR. *Sci. Rep.*, **6**, 21975.
33. Seelig, J., Nebel, S., Ganz, P., Bruns, C., (1993). Electrostatic and Nonpolar Peptide-Membrane Interactions - Lipid-Binding and Functional-Properties of Somatostatin Analogs of Charge Z = +1 to Z = +3. *Biochemistry*, **32**, 9714–9721.
34. Lai, A.L., Park, H., White, J.M., Tamm, L.K., (2006). Fusion peptide of influenza hemagglutinin requires a fixed angle boomerang structure for activity. *J. Biol. Chem.*, **281**, 5760–5770.
35. Seelig, J., (1997). Titration calorimetry of lipid-peptide interactions. *Biochim. Biophys. Acta, Mol. Cell. Res.*, **1331**, 103–116.
36. Li, Y., Han, X., Tamm, L.K., (2003). Thermodynamics of fusion peptide-membrane interactions. *Biochemistry*, **42**, 7245–7251.
37. Brittain, H.G., Richardson, F.S., Martin, R.B., (1976). Terbium(III) emission as a probe of calcium(II) binding sites in proteins. *J. Am. Chem. Soc.*, **98**, 8255–8260.
38. Lai, A.L., Freed, J.H., (2014). Influenza fusion peptide and transmembrane domain interaction induces distinct domains in lipid bilayers. *Biophys. J.*, **106**, 707a.
39. Kyte, J., Doolittle, R.F., (1982). A simple method for displaying the hydropathic character of a protein. *J. Mol. Biol.*,. https://doi.org/10.1016/0022-2836(82)90515-0.
40. Wimley, W.C., White, S.H., (1996). Experimentally determined hydrophobicity scale for proteins at membrane interfaces. *Nat. Struct. Biol.*, **3**, 842–848.
41. Vavrusova, M., Skibsted, L.H., (2013). Calcium binding to dipeptides of aspartate and glutamate in comparison with orthophosphoserine. *J. Agric. Food Chem.*,. https://doi.org/10.1021/jf400741e.
42. Tang, N., Skibsted, L.H., (2016). Calcium binding to amino acids and small glycine peptides in aqueous solution: Toward peptide design for better calcium bioavailability. *J. Agric. Food Chem.*, **64**, 4376–4389.
43. Belouzard, S., Millet, J.K., Licitra, B.N., Whittaker, G.R., (2012). Mechanisms of coronavirus cell entry mediated by the viral spike protein. *Viruses*, **4**, 1011–1033.
44. Millet, J.K., Whittaker, G.R., (2015). Host cell proteases: Critical determinants of coronavirus tropism and pathogenesis. *Virus Res.*,. https://doi.org/10.1016/j.virusres.2014.11.021.
45. Jing, Z., Liu, C., Qi, R., Ren, P., (2018). Many-body effect determines the selectivity for Ca2+ and Mg2+ in proteins. *Proc. Natl. Acad. Sci. U. S. A.*,. https://doi.org/10.1073/pnas.1805049115.
46. Bhalla, A., Chicka, M.C., Tucker, W.C., Chapman, E.R., (2006). Ca(2+)-synaptotagmin directly regulates t-SNARE function during reconstituted membrane fusion. *Nat. Struct. Mol. Biol.*, **13**, 323–330.
47. Brunger, A.T., (2005). Structure and function of SNARE and SNARE-interacting proteins. *Q. Rev. Biophys.*, **38**, 1–47.
48. Chicka, M.C., Hui, E., Liu, H., Chapman, E.R., (2008). Synaptotagmin arrests the SNARE complex before triggering fast, efficient membrane fusion in response to Ca2+. *Nat. Struct. Mol. Biol.*, **15**, 827–835.
49. Suarez, T., Gallaher, W.R., Agirre, A., Goni, F.M., Nieva, J. L., (2000). Membrane interface-interacting sequences within the ectodomain of the human immunodeficiency virus type 1 envelope glycoprotein: putative role during viral fusion. *J. Virol.*, **74**, 8038–8047.
50. Dubé, M., Rey, F.A., Kielian, M., (2014). Rubella virus: first calcium-requiring viral fusion protein. *PLoS Pathog.*, **10**, e1004530
51. Ge, M., Budil, D.E., Freed, J.H., (1994). ESR studies of spin-labeled membranes aligned by isopotential spin-dry ultracentrifugation: lipid-protein interactions. *Biophys. J.*, **67**, 2326–2344.
52. Ge, M. et al, (1999). Electron spin resonance characterization of liquid ordered phase of detergent-resistant membranes from RBL-2H3 cells. *Biophys. J.*, **77**, 925–933.
53. Ge, M. et al, (2003). Ordered and disordered phases coexist in plasma membrane vesicles of RBL-2H3 mast cells. An ESR study. *Biophys. J.*, **85**, 1278–1288.
54. Louis-Jeune, C., Andrade-Navarro, M.A., Perez-Iratxeta, C., (2012). Prediction of protein secondary structure from circular dichroism using theoretically derived spectra. *Proteins*, **80**, 374–381.